Soft Matter

Accepted Manuscript

This is an *Accepted Manuscript*, which has been through the Royal Society of Chemistry peer review process and has been accepted for publication.

Accepted Manuscripts are published online shortly after acceptance, before technical editing, formatting and proof reading. Using this free service, authors can make their results available to the community, in citable form, before we publish the edited article. We will replace this *Accepted Manuscript* with the edited and formatted *Advance Article* as soon as it is available.

You can find more information about *Accepted Manuscripts* in the Information for Authors.

Please note that technical editing may introduce minor changes to the text and/or graphics, which may alter content. The journal's standard Terms & Conditions and the Ethical guidelines still apply. In no event shall the Royal Society of Chemistry be held responsible for any errors or omissions in this *Accepted Manuscript* or any consequences arising from the use of any information it contains.

ROYAL SOCIETY OF CHEMISTRY

www.rsc.org/softmatter

Nanomechanics of Layer-by-Layer Polyelectrolyte Complexes: A Manifestation of Ionic Cross-links and Fixed Charges

Biao Han,[1] Daphney R. Chery,[1] Jie Yin,[2] X. Lucas Lu,[3] Daeyeon Lee,[4] Lin Han[1,]*

[1]*School of Biomedical Engineering, Science, and Health Systems, Drexel University, Philadelphia, PA 19104, United States*

[2]*Department of Mechanical Engineering, Temple University, Philadelphia, PA 19122, United States*

[3]*Department of Mechanical Engineering, University of Delaware, Newark, DE 19716, United States*

[4]*Department of Chemical and Biomolecular Engineering, University of Pennsylvania, Philadelphia, PA 19104, United States*

*Correspondence and requests for materials should be addressed to:

Dr. Lin Han

Phone: (215)571-3821

Fax: (215)895-4983

Email: lh535@drexel.edu.

For submission to *Soft Matter* as a *Full Paper*.

Soft Matter Accepted Manuscript

Abstract

This study investigates the roles of two distinct features of ionically cross-linked networks - ionic cross-links and fixed charges - in determining their nanomechanical properties. The layer-by-layer assembled poly(allylamine hydrochloride)/poly(acrylic acid) (PAH/PAA) network is used as the model material. The densities of ionic cross-links and fixed charges are modulated through solution pH and ionic strength (IS), and the swelling ratio, elastic and viscoelastic properties are quantified via an array of atomic force microscopy (AFM)-based nanomechanical tools. The roles of ionic cross-links are underscored by the distinctive elastic and viscoelastic nanomechanical characters observed here. First, as ionic cross-links are highly sensitive to solution conditions, the instantaneous modulus, E_0, exhibits orders-of-magnitude change upon pH- and IS-governed swelling, distinctive from the rubber elasticity prediction based on permanent covalent cross-links. Second, ionic cross-links can break and self re-form, and this mechanism dominates force relaxation of PAH/PAA under a constant indentation depth. At most states, degree of relaxation is > 90%, independent of ionic cross-link density. The importance of fixed charges is highlighted by the unexpected elastic nature of the network despite low ionic crosslink density at pH 2.0, 0.01M. Here, the complex is a net charged, loosely cross-linked, where the degree of relaxation is attenuated to ≈ 50% due to increased elastic contribution arising from fixed charge-induced Donnan osmotic pressure. In addition, this study develops a new method for quantifying the thickness of highly swollen polymer hydrogel films. It also underscores important technical considerations when performing nanomechanical tests on highly rate-dependent polymer hydrogel networks. These results provide new insights into the nanomechanical characters of ionic polyelectrolyte complexes, and lay the ground for further investigation of their unique time-dependent properties.

Keywords: ionic cross-links, fixed charges, polyelectrolytes, viscoelasticity, layer-by-layer assembly.

Soft Matter Accepted Manuscript

1. Introduction

Hydrogel networks formed by charged polyelectrolytes and connected by physical cross-links are distinct from covalent, non-ionic networks. The molecular-level distinction primarily lies in two characters, the presence of electrostatic interactions from uncompensated fixed charges and the breakable/recoverable nature of cross-links. These two characters are mainly responsible for their unique mechanical properties,[1-4] a wide range of stimulus-responsive physical properties, and in turn, various biomedical and engineering applications.[5] When physical networks are formed as nano-to-micrometer thick films, the reduced dimension renders great potential in applications that require rapid response time within seconds to minutes.[5] In many of these applications, such as cell substrates,[6-8] sensors and actuators,[9, 10] drug delivery,[11] anti-fouling[12], and tissue engineering,[13] understanding and controlling their mechanical properties is imperative for their successful utilization. For example, in cell culture, elastic modulus can strongly influence cell adhesion[14] and differentiation,[8, 15] primary cell phenotype[16] and stem cell lineage specification.[17] Recently, other mechanical factors, such as loss modulus,[18] stress relaxation patterns[19] and charge density[20] were also found to play important roles in regulating cell phenotype and activities.

Layer-by-layer (LbL) assembled polyelectrolyte complexes are one common type of such networks. In the past decade, there have been extensive studies on their mechanical properties. The instantaneous, elastic moduli were quantified by methods including quartz crystal microbalance (QCM),[21] instrumented nanoindentation,[22] strain-induced elastic buckling,[23] bulging test,[24] osmotic swelling,[25, 26] and atomic force microscopy (AFM)-nanoindentation on planar films[14, 27-37] or microcapsules.[38, 39] These studies showed that the elastic moduli are highly sensitive to post-assembly testing conditions, including solution bath pH,[27, 28] ionic strength (IS)[29-31] electrical field,[32, 33] and hydration energy of free counter-ions.[21] In the meantime, assembly conditions, such as assembly pH,[14, 34] IS,[29] additional covalent cross-linking[35, 36] and assembly sequence[37], also markedly affect the elastic modulus. Besides elasticity, time-dependent viscoelastic properties were also explored via whole film-level measurements such as piezo-rheometer,[40] dynamic uniaxial tensile tester,[41] capillary wave[42] and QCM with dissipation monitoring (QCM-D), [43] as well as localized AFM-

Soft Matter Accepted Manuscript

nanoindentation.[29, 38, 44-46] These whole-film measurements enabled direct quantification of the frequency-dependent storage and loss moduli, as well as time-dependent relaxation behaviors, while AFM was able to detect the local rate-dependence of modulus at nm-to-μm scale.[29, 44, 46] These studies provided a quantitative measure of the viscoelasticity in LbL films, and demonstrated the change in viscoelastic behaviors with the testing solution ionic strength.[31, 41]

Despite these efforts, there still lacks a mechanistic understanding regarding the nanomechanics of LbL films held by physical cross-links. In particular, it is unclear how the reversible nature of physical cross-links and the presence of fixed charges – the two distinct characteristics of ionically cross-linked networks – independently or cooperatively affect the stimulus-responsive mechanical properties of these LbL films. For example, for covalent networks, according to the theory of rubber elasticity,[47] there is a well-established inverse relation between the elastic modulus, E, and swelling ratio, v_s. Upon swelling, the permanent cross-link remain unchanged, the cross-link volume density scales inversely to v_s, and thus, $E \sim v_s^{-1/3}$.[48] For the ionically cross-linked networks, however, upon changes in solution environments, swelling/deswelling involves breaking and re-formation of ionic cross-links, as well as changes in its fixed charged density.[49-51] The rubber elasticity theory does not account for these changes, and the connection between swelling and mechanical properties is missing. Furthermore, for covalent networks, due to the permanence of cross-linking, time-dependent mechanics is governed by the polymer segmental motion,[52] as well as fluid flow-induced poroelasticity.[53] For ionic ones, as cross-links can break under stress and re-form by itself, the governing mechanisms can be markedly different. Also, the fixed charges on polymer chains could contribute to the elastic mechanics through Donnan osmotic swelling.[54] To date, this effect due to fixed charges has not been clearly elucidated. Without a fundamental understanding of these deterministic factors, it is difficult to quantitatively control the assembly and/or application environment to achieve the nanomechanical properties optimized for various applications.

The objective of this study is to uncover how the elastic and viscoelastic nanomechanical properties of LbL films are governed by ionic cross-links and fixed charges. For the films made of weak polyelectrolytes, these two factors can be controlled by the modulation of solution pH and IS. Toward this end, poly(allylamine

Soft Matter Accepted Manuscript

hydrochloride)/poly(acrylic acid) (PAH/PAA, **Fig. 1**a) LbL films are used as the model network. In aqueous solutions, the PAH/PAA network is connected by ionic pairs[55] between the protonated amine-groups of PAH (solution $pK_a \approx 10.5$ when in the form of PAH/PAA LbL films)[56] and charged carboxylate-groups of PAA ($pK_a \approx 2.3$ when in the form of PAH7.5/PAA3.5 LbL films).[49] The solution pH was varied between 2.0 and 5.5 to allow tuning of the ionization degree of PAA, while keeping PAH fully ionized. The film thus undergoes reversible swelling/de-swelling upon changes in pH, switching between being highly cross-linked, net neutral (higher pH) and loosely linked, net charged (lower pH) (Fig. 1b). [49] In addition, the solution IS was varied between 0.01M to 1.0M to allow tuning of cross-link density and electrostatics. In net neutral states, IS influences the cross-link without affecting the charged nature of polymers through the "doping" effect.[50] In net charged states, IS tunes the magnitude of electrostatic interactions via Debye screening.[54]

To achieve our goal, an array of atomic force microscopy (AFM) tests were developed and applied to assess the film thickness, instantaneous indentation modulus and viscoelastic force relaxation in monovalent NaCl solutions. The experimental results were interpreted through elastic and viscoelastic contact mechanics models to extract material properties including instantaneous and equilibrium moduli, as well as relaxation time constants. As a result, this study provides the first experimental evidence that highlights the unique elastic and viscoelastic features of PAH/PAA endowed by fixed charges and ionic cross-linking. Through tuning each factor of pH or IS while maintaining the other at constant, this study is the first to de-convolute the contribution of each factor. The breakable and reversible nature of ionic cross-links is found to result in a highly environment-sensitive, viscoelastic nature of the network that is distinctive from covalent networks. On the other hand, the presence of fixed charges leads to an unexpected more elastic nature at the net charged state, despite having the lowest cross-link density. These properties are expected to provide insights into the mechanics of physically cross-linked hydrogel networks in general, and render necessary benchmark for designing mechanics-based applications of stimulus-responsive materials.

2. Materials and Methods

2.1 Sample preparation

Soft Matter Accepted Manuscript

Poly(allylamine hydrochloride) (PAH, $M_w \approx$ 120,000-200,000, Alfa Aesar, Ward Hill, MA) and poly(acrylic acid) (PAA, $M_w \approx$ 100,000, Sigma-Aldrich, St. Louis, MO) were used as received. Following previously established procedures,[22] the 50-bilayer, ionically cross-linked PAH/PAA multilayer films, $(PAH7.5/PAA3.5)_{50}$, were prepared via layer-by-layer (LbL) assembly in 0.01M polyelectrolyte deionized water solutions (repeat unit concentration) at pH 7.5 for PAH, and 3.5 for PAA, respectively. The pH of assembly solution was adjusted by adding HCl or NaOH. With a total of 100 building layers, PAA was the top layer of the film to ensure a hydrophilic nature on the surface.[57] The use of a 50-bilayered film is to minimize the effects of substrate constraints and non-linearity in mechanical properties at large deformation strains. The LbL assembly was carried out on freshly Piranha solution-cleaned glass slides via a programmable slide stainer (HMS, Zeiss, Peabody, MA) at room temperature. The films were then air dried and stored for < 48 hours before tests.

2.2 Film thickness measurement

Two AFM-based modalities were used to measure the film thickness, H, after selective film removal. First, for $H \leq 10$ μm, contact mode AFM imaging[58] (Dimension Icon, BrukerNano, Santa Barbara, CA) was used (**Fig. 2**a, method I). This method was applied to films at the dry state and at the less swollen states in solution (pH ≥ 3.0, Fig. 2b). When H is comparable or greater than 10 μm, due to the limit of AFM z-piezo (~10 μm for Dimension Icon AFM),[59] contact mode imaging is not applicable. A new "z-motor assisted" method employing both the z-piezo and z-step motor was developed to quantify H (Fig. 2a, method II; a detailed description of the potential application of this method is provided in ESI, Appendix A1). First, the AFM tip was placed over the film. When the AFM system was engaged at a pre-set indentation force, F_0 (≈ 3 – 5 nN), the movement of z-step motor onto the film was recorded as z_1. After retraction of the tip to its original location, the tip was laterally moved to the substrate region where the polymer film was removed. The same procedure was repeated to record the motor movement, z_2. At the pre-set force F_0, the indentation depth was measured as D_0 by nanoindentation (as discussed in details later). The thickness H was thus calculated as $H = z_2 - z_1 + D_0$. This method was validated on micro-fabricated Si substrates with 5-μm height steps, as well as direct comparison of

Soft Matter Accepted Manuscript

PAH/PAA in the states where $H \approx 5 - 10$ μm (e.g., pH = 3.0 and IS = 0.1 M, Fig. 2c). When validated on micro-fabricated Si substrates with spatial resolution of the AFM *z*-step motor is 100 nm,[59] the systematic error is < 1% when $H > 10$ μm (Fig. 2c). This LbL film has an as-assembled dry thickness of 3.35 ± 0.01 μm (mean ± SEM, n = 48, Fig. 2d), assessed by contact mode AFM imaging. Accordingly, the volume swelling ratio v_s is thus calculated as (Fig. 2d),

$$v_s = \frac{H_{wet} - H_{dry}}{H_{dry}} \times 100\% .$$

2.3 AFM-based nanoindentation and force relaxation

AFM-based nanoindentation and ramp-and-hold force relaxation experiments were performed in the indenter mode of the 3D Molecular Force Probe (MFP-3D, Asylum Research, Santa Barbara, CA). The microspherical indenter tip was prepared by attaching one polystyrene colloid ($R_{tip} \approx 12.5$ μm, elastic modulus is ~ 4 GPa,[60] infinite compared with that of PAH/PAA, Polysciences, Warrington, PA) onto a tipless cantilever (nominal spring constant k = 5.4 N/m, NSC35/Cr-Au, cantilever C, NanoAndMore, Lady's Island, SC) by M-Bond 610 epoxy (Polysciences) using the optical microscope and *z*-step motor of the Dimension Icon AFM. Depth-controlled nanoindentation was conducted at a constant loading/unloading indentation rate, v_D = 5 μm/s, up to a maximum indentation force ≈ 1 μN using the MFP-3D. During the indentation, the *z*-piezo ramp velocity was continuously adjusted in the indenter mode to maintain this constant indentation depth rate. For the relaxation test, immediately following the indentation, the force was measured as a function of time during the 30 seconds hold period. The indentation depth was kept constant by adjusting the *z*-piezo position in the indenter mode to compensate for the reduction in cantilever bending due to force relaxation. All of the experiments were performed in pH = 2.0 – 5.5, IS = 0.01 – 1.0 M NaCl solutions. For each IS, pH was adjusted by adding HCl while reducing the concentration of NaCl to maintain constant IS. Experiment at each IS and pH combination was repeated on at least 10 locations on each of the 3 samples. The data from each sample were pooled since no statistical differences were found across these samples ($p > 0.05$ via Kruskal-Wallis test for each pH and IS).

Soft Matter Accepted Manuscript

As the nanomechanical properties of PAH/PAA are highly rate-dependent, to demonstrate the necessity of maintaining constant indentation rate during indentation, and constant depth during force relaxation, two sets of open-loop control experiments were performed at pH 5.5 and 2.0, IS = 0.01M. During the open-loop indentation, the *z*-piezo displacement velocity, instead of indentation rate, was kept constant, whereby the indentation rate varied due to increased cantilever bending. During the open-loop force relaxation, the *z*-piezo displacement, instead of indentation depth, was kept constant, whereby the indentation depth, D, also varied due to changes in cantilever bending. A detailed description of technical considerations in AFM-based nanomechanical studies of highly rate-dependent polymer networks is provided in the ESI (Appendix A2).

2.4 Data analysis

For each indentation location, the indentation force versus depth (*F*-*D*) curve was obtained by calibrating the cantilever deflection sensitivity on a mica substrate, and actual spring constant via the thermal oscillation method,[61] respectively. For each *F*-*D* curve, the tip-sample effective contact point was determined via an algorithm developed previously for soft materials in the absence of attractions.[62, 63] The effective instantaneous indentation modulus, E_0, was calculated by fitting the whole loading portion of each curve to the linear elastic Hertz model with finite thickness correction via least squares linear regression (LSLR),

$$F = \frac{4}{3}\frac{E_0}{\left(1-\nu^2\right)} R_{tip}^{1/2} D^{3/2} C_\chi\left(F, D, H, R\right),$$

where ν is the Poisson's ratio (≈ 0.49 for highly swollen hydrogels),[64] R_{tip} is the tip radius, and C_χ is the substrate constraint correction factor that depends on F, D, H and R_{tip}.[65] Here, E_0 represents the instantaneous modulus measured at the constant indentation rate of υ_D = 5 μm/s.

During the force relaxation, the deflection and *z*-piezo displacement were recorded as a function of time at a sampling rate of 2 kHz. At each time point, the temporal modulus, $E(t)$, was calculated by fitting $F(t)$ and D to the substrate-corrected Hertz model, whereby D was constant during the relaxation. To quantitatively elucidate the viscoelastic force relaxation behavior, the five-element SLS model[66] was applied to each curve,

Soft Matter Accepted Manuscript

$$E_0 = E_\infty + E_1 \exp\left(-\frac{t}{\tau_1}\right) + E_2 \exp\left(-\frac{t}{\tau_2}\right)$$

where E_∞ is the equilibrium modulus, E_1 and E_2 are the moduli corresponding to the two relaxation time constants, τ_1 and τ_2, respectively ($E_1 > E_2$). This five-element model was chosen since it requires minimum number of parameters to adequately describe the relaxation (coefficient of determination, $R^2 > 0.94$ for all fits), while the simpler three-element model with one time constant cannot explain the relaxation patterns. The fit was conducted via the nonlinear fitting tool based on the Levenberg-Marquardt Algorithm (LMA) in Matlab, whereby the boundary condition was set as $E_0 = E_\infty + E_1 + E_2$ at $t = 0$, and the initial fitting condition was set as $E_1/E_0 = 0.85$, $E_2/E_0 = 0.1$, $\tau_1 = 0.05$ sec, and $\tau_2 = 2$ sec, respectively.

3. Results

The film thickness, H, and associated degree of swelling, v_s, were quantified via contact mode AFM imaging and z-motor method (Fig. 2a-c). Solution pH and IS were found to synergistically modulate the values of H and v_s, as shown in Fig. 2d. In the tested range of IS, values of film thickness at pH ≥ 3.5 were at their minima, close to those measured under dry conditions ($v_s \approx 20 – 35\%$). At pH < 3.5, the film underwent substantial swelling, at all tested IS. Specifically, at 0.01M IS, film thickness increased when lowering pH from 3.5 to 2.0, reached a maximum of 17.3 ± 0.8 μm (v_s = 429 ± 34 %) before the film dissolved at pH < 2.0. At higher IS of 0.1M and 1.0M, while its trend of pH-dependence was similar to that at 0.01M, the film thickness decreased with increasing IS. In addition, the pH thresholds of film swelling and dissolving were also affected by IS. At 0.1M, the film started significant swelling at pH = 3.0, and dissolved at pH < 2.5. In comparison, at 1.0M, the film started to swell at pH = 2.5, but quickly dissolved at pH < 2.5.

The instantaneous modulus, E_0, was calculated by applying the substrate-corrected Hertz model to the whole loading portion of *F-D* curves,[65] shown as the curves in four representative states (**Fig. 3**a). Similar to swelling, values of E_0 also exhibited marked pH- and IS-dependence (Fig. 3b). At each IS, E_0 retained at a similar magnitude at pH ≥ 3.5, but decreased up to two orders during swelling at pH < 3.5. Interestingly, at pH

Soft Matter Accepted Manuscript

≥ 3.5, in contrast to the lack of sensitivity in film thickness to solution IS (Fig. 2d), we detected a ten-fold difference in E_0 across the tested IS. On the other hand, at pH < 3.5, the overall decreasing trend in modulus was in alignment with the increase in swelling at all IS, although the magnitude change in modulus was much greater than the thickness. In addition, at pH = 3.0, E_0 was significantly lower than at its adjacent pH conditions (2.5 and 3.5) at both 0.01M and 0.1M, but not at 1.0M. The relationship between swelling ratio and instantaneous modulus is further highlighted in the three representative states summarized in **Fig. 4**.

In contrast to the marked variation of film thickness and instantaneous modulus with pH and IS shown in Figs. 2 and 3, viscoelastic force relaxation patterns were similar across a wide range of tested states. Based on the five-element SLS model shown in **Fig. 5**a (see Materials and Methods for detailed description), the equilibrium modulus, E_0, and two viscoelastic relaxation modes, (E_1, τ_1) and (E_2, τ_2), were extracted (Fig. 5b). The degree of relaxation, denoted as ($1 - E_\infty/E_0$), was > 95% at all states of pH ≥ 3.0 (**Fig. 6**a). In addition, as shown by the same data replotted against film thickness, H (Fig. 6b), and instantaneous modulus, E_0 (Fig. 6c), the relaxation trend was independent of these two parameters at pH ≥ 3.0. At 0.01M and 0.1M, under the near dissolution pH of 2.5, the relaxation degree was modestly lower (≈ 90%). From the five-element SLS model fit, two relaxation time constants and moduli were calculated at each state, corresponding to two different governing mechanisms, as will be discussed later in detail. Across these states, the relaxation was found to be dominated by the short-term relaxation mode (E_1, τ_1), whereby E_1 accounted for ≥ 70% of E_0 (**Fig. 7**a). The short-term time constant, τ_1, exhibited only minor variations between 25 ± 5 msec (pH 3.0, 0.01M) and 46 ± 9 msec (pH 5.5, 0.01M) (Fig. 7b). This domination was present also for the two near dissolution states at higher IS (pH 2.5, 0.1M and 1.0M, Fig. 7a,b), as the results suggested a minor role of elastic modulus (E_∞/E_0 < 10%, Fig. 6a), and major contribution of E_1 (E_1/E_0 > 70%, Fig. 7a). In contrast, the long-term relaxation mode only contributes to ≤ 20% of E_0 (E_2/E_0, Fig. 7c), and with larger variations in τ_2 across all the states (Fig. 7d).

At pH 2.0, 0.01M, at the most swollen state with lowest instantaneous modulus, the relaxation behavior of PAH/PAA was found to be much more elastic, as shown in Figs. 6 and 7. The degree of relaxation was attenuated to 50.9 ± 2.5% (Fig. 6a). According to the five-element SLS model, the short term relaxation (E_1, τ_1)

Soft Matter Accepted Manuscript

also had a much smaller contribution to the overall modulus, $E_1/E_0 = 36.5 \pm 1.5\%$ (Fig. 7a). The time constant, τ_1, was also found to be significantly longer compared with other pH and IS states (Fig. 7b). On the other hand, similar to other states, the long term relaxation played a relatively minor role ($E_2/E_0 = 12.6 \pm 1.6\%$, Fig. 7c).

4. Discussion

Based on the pH- and IS-dependent swelling and mechanical properties of PAH/PAA, we report novel findings on the molecular mechanisms that govern the nanomechanics of ionically cross-linked polyelectrolyte networks. The roles of ionic cross-links and fixed charges are de-convoluted through the modulation of pH and IS. First, the relations between modulus and swelling ratio of PAH/PAA are different from the prediction by rubber elasticity theory, and show direct impacts of the stimulus-responsive nature of ionic cross-links. The importance of fixed charges in the instantaneous modulus is highlighted by the substantial pH-governed swelling (Fig. 2d), as well as IS-dependence of E_0 in the charged state (Fig. 3b). Second, the viscoelastic force relaxation is shown to be largely dominated by the localized breaking and re-formation of ionic cross-links, a mechanism distinctive from the chain conformation-governed relaxation. Third, the roles of fixed charges are highlighted by the unexpectedly stronger elastic response at the highly net charged state of pH 2.0, 0.01M (Fig. 6a). When the Donnan osmotic swelling effect arising from fixed charges results becomes important, the network behaves much more elastically despite having the lowest cross-link density.

4.1 Roles of stimulus-responsive ionic cross-links in swelling and instantaneous modulus

The stimulus-responsive nature of ionic cross-links is illustrated by the pH- and IS-dependence of thickness H (Fig. 2d) and instantaneous modulus E_0 (Fig. 3b). Specifically, the swelling-mechanics behavior that is unique compared with that of covalent networks can be highlighted by three representative states in Fig. 4. First, the ten-fold (1.0M) to hundred-fold (0.1 and 0.01M) decrease in E_0 during pH-induced swelling is different from covalent networks, in which cross-links stay permanent during swelling. According to the rubber elasticity theory,[47] the conformational entropy-governed elastic modulus scales with $v_s^{-1/3}$.[48] For example, when a covalent network swells at a ratio equivalent to that of PAH/PAA from pH 5.5 to 2.0 at 0.01M (3.2 ± 0.1 ×,

Soft Matter Accepted Manuscript

Fig. 4a), a 68.9 ± 0.3% reduction in v_s, and thus, a 32.3 ± 0.2% decrease in E_0 is expected (Fig. 4b). For polymer films end-grafted to a planar substrate, this reduction could be attenuated by the internal compressive stress built upon substrate-constrained swelling.[67, 68] In contrast, upon swelling, PAH/PAA experiences major loss in the amine-carboxylate paired ionic cross-links. This effect leads to the observed orders-of-magnitude decrease in E_0 that far exceeds the prediction by rubber elasticity[47] (Fig. 4b). In addition, for weak polyelectrolyte networks such as PAH/PAA, there is a secondary effect that can increase E_0 when lowering pH (< 3.0). As the protonation of carboxylic acid groups increase the number of uncompensated amine groups (i.e., fixed charges), additional osmotic pressure arising from net positive charge can contribute to an increase in elastic modulus.[54, 69] However, this effect is expected to be much weaker than the loss in cross-links, and does not appear to reverse the decreasing trend of E_0 as pH decreases.

Second, the reduction of E_0 upon de-swelling when increasing IS at net neutral states (pH ≥ 3.5, Fig. 3) also does not conform to the rubber elasticity theory. For example, at pH 5.5, PAH/PAA undergoes moderate de-swelling when increasing IS from 0.01M to 1.0M (Fig. 4a). However, instead of experiencing an increase in E_0, as would be predicted by rubber elasticity, E_0 decreases for approximately ten-fold (Fig. 4b). Under these net neutral states, compensation of fixed charges is achieved through both "intrinsic" pairing between opposite fixed charges on polymer chains, and "extrinsic" pairing between fixed charges and free counter-ions.[50, 70] Ionic cross-links in PAH/PAA can only form between the intrinsic carboxylate-amine pairs. At a higher concentration of free ions, there is an increased portion of extrinsic ionic pairing, i.e., pairing between the carboxylate or amine groups and free counter ions (H^+, Na^+, Cl^- here) (Fig. 1b), and in turn, a decreased portion of intrinsic pairing.[31] Increasing IS thus effectively reduces ionic cross-link density, namely the "doping" effect,[50] as highlighted by the IS-governed modulus decrease when increasing IS at pH 5.5 (Fig. 4).

Interestingly, across the three representative states shown in Fig. 4, the influence of pH appears to be much stronger on both the degree of swelling and modulus than that of IS. This is because, as discussed previously, pH directly determines the density of molecular sites available for ionic cross-link formation (the charged carboxyl groups here), while IS mainly plays a regulatory role by impacting the likelihood of these

Soft Matter Accepted Manuscript

available sites in forming cross-links. In addition, pH also results in the substantial swelling at pH = 2.0, 0.01M (state *A* in Fig. 4) through the osmotic swelling effect, whereas this effect is negligible at the two net neutral states of *B* and *C* used to illustrate the impacts of IS in Fig. 4.

4.2 Roles of fixed charges in swelling and instantaneous modulus

The impacts of fixed charges on nanomechanics can be extracted, and differentiated from the contributions by ionic cross-links based on the swelling and mechanical behaviors at net charged states. First, the marked swelling (Fig. 2d) at low pH ≤ 3.0, is dominated by the effects of increased fixed charge density. The increased osmotic pressure exerted by the net positive charges of unpaired amine groups on PAH and associated re-distribution of free ions lead to substantial swelling in a typical Donnan equilibrium (Fig. 1b),[71] similar to the trend previously observed on end-grafted polyelectrolyte monolayers.[72, 73] A more swollen, new equilibrium state is reached when a balance between the Donnan osmotic swelling and resistance to further polymer stretching due to loss in conformational entropy is reached. In the meantime, protonation of carboxylate groups upon lowering pH also leads to a marked decrease in ionic cross-link density. However, the impacts of cross-link loss on swelling are very minor. As discussed previously, increasing IS from 0.01M to 1.0M also results in appreciable loss in ionic cross-links due to the "doping" effect.[50] However, this effect leads to a marginal decrease in film thickness, *H*, rather than an increase (Fig. 2d).

The contribution of osmotic pressure exerted by the net positive fixed charges to mechanics is highlighted by the IS-dependence of E_0.[74] According to the Donnan equilibrium, osmotic pressure due to the asymmetric distribution in free counter-ions versus co-ions is largely attenuated at higher IS.[75] At the nanoscale, Donnan equilibrium can also be more precisely described in the context of electrical double layer (EDL) repulsion by the Poisson-Boltzmann theory.[54] This effect is quantitatively depicted by the Debye screening length, κ^{-1}, the distance whereby local electrical potential from one point charge decreases to $1/e$ of its original magnitude.[54] Osmotic forces can contribute to compressive modulus if the average fixed charge-charge distance, l_c is less than or comparable to κ^{-1}. In monovalent electrolyte solutions, $\kappa^{-1} = \sqrt{\varepsilon RT / 2F^2 c_0}$, where ε is the

Soft Matter Accepted Manuscript

permittivity of the network medium at room temperature, R is the universal gas constant, T is the absolute temperature in K, F is the Faraday constant (96,500 C/mol), and c_0 is the ionic strength of the medium. If the permittivity of water is used as a first-level approximation, $\varepsilon_W = 6.92 \times 10^{-10}$ C/(N·m^2), κ^{-1} is calculated as 3 nm, 1 nm and 0.3 nm at IS = 0.01M, 0.1M, and 1.0M, respectively. According to PAH monomer configuration, the closest distance between adjacent amine groups on PAH is ≈ 0.46 nm, calculated in ChemBio3D (PerkinElmer, Waltham, MA). The average charge distance, l_c, is greater than this theoretical minimum value, since not all PAH amine groups are charged, and a portion of charged groups is compensated by the carboxyl groups and free counter-ions (Fig. 1b). It is thus reasonable to expect $l_c > \kappa^{-1}$ at 1.0M, and it is possible $l_c \leq \kappa^{-1}$ at 0.01M and 0.1M. Under this scenario, the contribution of EDL repulsion to E_0 is expected to be appreciable at lower IS, but negligible at 1.0M. Taken together both effects, at the same pH, E_0 is higher at lower IS, likely owing to the presence of higher ionic cross-link density and greater osmotic pressure (Fig. 3). Our ongoing studies using the attenuated total reflectance-infrared spectroscopy (ATR-FTIR)[76] aims to determine the charge density with the PAH/PAA complex, and thus, will provide a quantitative assessment to the observed IS-dependence of E_0.

The presence of fixed charges appears to also affect the IS-dependent dissolution pH threshold of PAH/PAA. At IS = 0.01M, the film starts swelling at pH < 3.5, and dissolves at pH < 2.0 when most carboxyl groups are protonated (Fig. 2d). In contrast, at 1.0M, the swelling starts at pH 2.5, close to the bulk pK_a of PAA ≈ 2.3,[49] and soon dissolves at pH < 2.5 (Fig. 2d). According to the Poisson-Boltzmann theory, and its continuum-level approximation, the Donnan equilibrium,[54] local concentration of H^+ within PAH/PAA is lower than the bulk due to the presence of fixed positive charges. The local pH in the PAH/PAA complex is thus higher, and this difference is greater at lower IS. As a result, in the presence of fixed positive charges, the bulk pKa for the dissolving threshold of PAA is further reduced at lower IS.[56]

Another impact of fixed charges on E_0 is demonstrated by the increase in instantaneous modulus from pH 3.0 to 2.5 at IS = 0.01M and 0.1M (Fig. 3b), despite expected loss in ionic cross-links and significant swelling (Fig. 2d).[31] A possible explanation is that the increase in net charge density reaches a threshold whereby l_c becomes less than or comparable to κ^{-1}. As a result, the increase in E_0 due to osmotic pressure

Soft Matter Accepted Manuscript

overweighs the impacts of ionic cross-link loss from pH 3.0 to 2.5. This hypothesis is partly supported by the fact that this self-stiffening swelling is absent at 1.0M IS, where the contribution of osmotic pressure is negligible.

4.3 Viscoelastic relaxation mechanisms arising from ionic cross-links and fixed charges

Force relaxation test results (Fig. 5) underscore the novel viscoelastic characteristics of PAH/PAA, which is endowed by the breakable and recoverable nature of ionic cross-links, and its cross-talk with fixed charges. For covalent networks, viscoelastic force relaxation is mainly governed by the conformational change, reptation and disentanglement of polymer chain segments, whereby cross-links remain unaffected.[77] Therefore, the degree of relaxation decreases with increasing cross-link density due to stronger hindrance to polymer segmental motion.[78] In contrast, in PAH/PAA, ionic cross-links can reversibly break and re-form under external stresses.[3, 79] This time-dependent mechanism takes place at the localized sites of each amine-carboxylate ionic pair. It is thus likely not directly governed by the polymer chain segmental motion. The cross-link density-regulated segmental motion hindrance can thus have much less influence on relaxation. Indeed, in this study, the independence of force relaxation degree ($1 - E_\infty/E_0 \geq 0.95$) on H (Fig. 6b) or E_0 (Fig. 6c) across a wide range of states at pH $\geq$ 3.0. As PAH/PAA is purely held by ionic cross-links, this nearly 100% relaxation provides a direct, strong evidence that ionic cross-link breaking and re-formation dominate the viscoelasticity of ionic networks.

At net charged states, there is an increased portion of elasticity, evidenced by the reduced degree of relaxation, ($1 - E_\infty/E_0$) (Fig. 6a). At pH 2.5, 0.1M and 1.0M, ($1 - E_\infty/E_0$) is modestly lower ($\approx$ 90%) than that of higher pH, net neutral states. Under these two conditions, the network becomes much more swollen (Fig. 6b) and net charged. Upon the drastic loss of ionic cross-links, polymer chain segmental length between adjacent cross-links increases. For these loosely bound networks, it is possible that the polymer conformational entropy-driven elasticity can play a modest role in the overall modulus. In addition, osmotic pressure arising from fixed charges may also contribute to elasticity,[80] but this effect is minor at higher IS.

Soft Matter Accepted Manuscript

The impacts of fixed charges on viscoelasticity are best illustrated by the unexpected, more elastic nature at pH 2.0, 0.01M (Fig. 6a). At this state, PAH/PAA is highly charged, loosely cross-linked, and has the lowest instantaneous modulus E_0 (Fig. 6b,c). Since the modulus of hydrogel networks scales with cross-link density, networks with lower modulus are expected to undergo more viscoelastic relaxation due to reduced hindrance in chain segmental motion. In contrast, an opposite trend is observed on PAH/PAA here, as is most likely due to the increased contribution of osmotic pressure to elasticity,[80] given the Debye length, $\kappa^{-1} \approx 3$ nm > l_c. At this state, owing to both the increased elastic osmotic pressure and marked reduction in the overall modulus ($E_0 = 0.091 \pm 0.013$ MPa), the relative contribution of elasticity to E_0 becomes much more substantial, and thus, the weight of cross-link breaking and re-formation governed relaxation is reduced (Figs. 5b and 6).

4.4 Viscoelastic relaxation time constants and modes

Across a wide range of pH and IS states, the domination of short term relaxation (E_1/E_0), and its insensitivity to film thickness and modulus (Fig. 7) is also different from the viscoelastic relaxation of covalent networks, which is strongly regulated by cross-link density.[81] The lack of cross-link density dependence again confirms that the short term relaxation is mostly governed by mechanisms independent of cross-link density, i.e., breaking and re-formation of ionic cross-links. Domination of this mode in the overall modulus also supports the hypothesis that cross-link breaking and re-formation is the major viscoelasticity mechanism with a time constant ≈ 35 msec (average τ_1 across pH = 2.5 – 5.5 at all IS). The less important long term relaxation possibly involves several viscoelastic mechanisms that take place synergistically, including polymer chain conformational change, reptation and disentanglement, fluid flow as well as cross-link breaking and re-formation.[52] With the current experimental set-up, roles of individual mechanism cannot be directly de-convoluted. However, since the contribution of E_2 to E_0 is marginal (Fig. 7c), the cross-link breaking and re-formation mechanism that governs τ_1 can be regarded as the dominating viscoelasticity mechanism overall. Lastly, these results together suggest that for ionic networks, since cross-links can break and re-form during relaxation, it is the instantaneous modulus, E_0, instead of the equilibrium modulus, E_∞, that better represents the cross-link density at the initial, un-deformed state.

Soft Matter Accepted Manuscript

Similar to the scenario of E_∞/E_0 (Fig. 6a), at pH 2.0, 0.01M, the lower ratio of E_1/E_0 (Fig. 7a), and significantly longer τ_1 (Fig. 7b) suggest that cross-link breaking and re-formation is likely not the only mechanism governing this relaxation. At this highly swollen, loosely bound state, PAH/PAA adopts much longer segmental chain length between adjacent cross-links, and with a higher water content (80.4 ± 0.1 % calculated based on the dry versus wet *H*) (Fig. 1b). It is possible for other time-dependent modes, such as chain segmental motion and fluid flow to have a more appreciable role in the relaxation corresponding to τ_1. In particular, given the high water content, fluid flow-induced poroelasticity could be an important factor in both short and long term force relaxation.[63] Ongoing studies are using our custom-built, AFM-based dynamic oscillatory nanorheometer[63, 82, 83] to de-convolute the roles of intrinsic viscoelastic modes and fluid flow-induced water-polymer interactions.

5. Conclusions

In this study, using PAH/PAA LbL films, we revealed the roles of two distinct molecular characteristics of ionically cross-linked networks, ionic cross-links and fixed charges, in their elastic and viscoelastic nanomechanical properties. The stimulus-responsive nature of ionic cross-links held by the amine-carboxylate ionic pairing endows the network with a swelling-mechanics relationship that cannot be explained by the rubber elasticity theory based on the permanence of covalent cross-links. Furthermore, from the force relaxation tests, viscoelasticity is found to be dominated by the localized breaking and re-formation of ionic cross-links. The time-dependent relaxation pattern exhibits a consistent time constant τ of a 35 millisecond across most pH and IS states, independent of cross-link density or degree of swelling. One exception is found at pH 2.0, 0.01M, where osmotic pressure from fixed charges leads to a more elastic response with longer relaxation time constants. As the mechanical properties of non-covalently cross-linked networks is key to realize their wide biomedical and engineering applications, we expect this study to provide a fundamental knowledge base that enables a better informed design of their mechanics-based applications.

Our ongoing studies on ionically cross-linked networks aim to quantitatively explain the origins of the viscoelasticity of ionic networks, and to de-convolute different time-dependent mechanisms. We are using

Soft Matter Accepted Manuscript

ATR-FTIR[76] to measure the pH and IS-dependent fixed charge density and ionic cross-link density. The nanomechanical properties will be interpreted based on these results as well as the rubber elasticity[47] and Donnan equilibrium theories[75] to connect the elastic and viscoelastic properties with their molecular states. In addition, we are studying force relaxation and creep of PAH/PAA under intermittent loading to further probe into the unique viscoelastic nature of ionic networks. Through employing our recently developed AFM-nanorheometer,[63, 82, 83] we are de-convoluting the fluid flow-governed poroelasticity from the intrinsic viscoelasticity of these networks. We expect these studies on the pure ionic network of PAH/PAA will lay the ground for revealing the mechanical and electromechanical characters of more complicated hydrogel networks, such as inter-penetrating networks[84] and extracellular matrices of biological tissues.[85]

Electronic Supplementary Information

Additional technical discussions on the film thickness measurement (Appendix A1) and AFM-based nanomechanical studies of highly rate-dependent polymer networks (Appendix A2) are provided in the ESI.[86-91]

Acknowledgement

This work was supported by the Faculty Start-up Grant at Drexel University (LH), the Faculty Start-up Grant at Temple University (JY), and NSF DMR-1055594 (DL). We thank Dr. Christopher Y. Li for valuable discussions. We also thank the Nano/Bio Interface Center at the University of Pennsylvania for the use of MFP-3D.

Soft Matter Accepted Manuscript

References

1. T. L. Sun, T. Kurokawa, S. Kuroda, A. Bin Ihsan, T. Akasaki, K. Sato, M. A. Haque, T. Nakajima and J. P. Gong, *Nat. Mater.*, 2013, **12**, 932-937.
2. J.-Y. Sun, X. Zhao, W. R. K. Illeperuma, O. Chaudhuri, K. H. Oh, D. J. Mooney, J. J. Vlassak and Z. Suo, *Nature*, 2012, **489**, 133-136.
3. X. Zhao, N. Huebsch, D. J. Mooney and Z. Suo, *J. Appl. Phys.*, 2010, **107**, 063509.
4. K. J. Henderson, T. C. Zhou, K. J. Otim and K. R. Shull, *Macromolecules*, 2010, **43**, 6193-6201.
5. M. A. Cohen Stuart, W. T. S. Huck, J. Genzer, M. Müller, C. Ober, M. Stamm, G. B. Sukhorukov, I. Szleifer, V. V. Tsukruk, M. Urban, F. Winnik, S. Zauscher, I. Luzinov and S. Minko, *Nat. Mater.*, 2010, **9**, 101-113.
6. A. J. Engler, L. Richert, J. Y. Wong, C. Picart and D. E. Discher, *Surf. Sci.*, 2004, **570**, 142-154.
7. D. E. Discher, D. J. Mooney and P. W. Zandstra, *Science*, 2009, **324**, 1673-1677.
8. K. Ren, T. Crouzier, C. Roy and C. Picart, *Adv. Funct. Mater.*, 2008, **18**, 1378-1389.
9. D. Mertz, J. Hemmerlé, J. Mutterer, S. Ollivier, J.-C. Voegel, P. Schaaf and P. Lavalle, *Nano Lett.*, 2007, **7**, 657-662.
10. S.-W. Lee, J. H. Prosser, P. K. Purohit and D. Lee, *ACS Macro Lett.*, 2013, **2**, 960-965.
11. K. C. Wood, J. Q. Boedicker, D. M. Lynn and P. T. Hammond, *Langmuir*, 2005, **21**, 1603-1609.
12. S. Y. Wong, L. Han, K. Timachova, J. Veselinovic, M. N. Hyder, C. Ortiz, A. M. Klibanov and P. T. Hammond, *Biomacromolecules*, 2012, **13**, 719-726.
13. C. J. Detzel, A. L. Larkin and P. Rajagopalan, *Tissue Eng. B Rev.*, 2011, **17**, 101-113.
14. M. T. Thompson, M. C. Berg, I. S. Tobias, M. F. Rubner and K. J. Van Vliet, *Biomaterials*, 2005, **26**, 6836-6845.
15. A. D. Augst, H. J. Kong and D. J. Mooney, *Macromol. Biosci.*, 2006, **6**, 623-633.
16. M. D. Moussallem, S. G. Olenych, S. L. Scott, T. C. S. Keller, III and J. B. Schlenoff, *Biomacromolecules*, 2009, **10**, 3062-3068.
17. A. J. Engler, S. Sen, H. L. Sweeney and D. E. Discher, *Cell*, 2006, **126**, 677-689.
18. A. R. Cameron, J. E. Frith and J. J. Cooper-White, *Biomaterials*, 2011, **32**, 5979-5993.
19. O. Chaudhuri, L. Gu, M. Darnell, D. Klumpers, S. A. Bencherif, J. C. Weaver, N. Huebsch and D. J. Mooney, *Nat. Commun.*, 2015, **6**, 6365.
20. Y. M. Chen, R. Ogawa, A. Kakugo, Y. Osada and J. P. Gong, *Soft Matter*, 2009, **5**, 1804-1811.
21. M. Salomäki, T. Laiho and J. Kankare, *Macromolecules*, 2004, **37**, 9585-9590.
22. P. V. Pavoor, A. Bellare, A. Strom, D. Yang and R. E. Cohen, *Macromolecules*, 2004, **37**, 4865-4871.
23. A. J. Nolte, M. F. Rubner and R. E. Cohen, *Macromolecules*, 2005, **38**, 5367-5370.
24. C. Jiang, S. Markutsya, Y. Pikus and V. V. Tsukruk, *Nat. Mater.*, 2004, **3**, 721-728.
25. B. S. Kim, T. H. Fan, O. V. Lebedeva and O. I. Vinogradova, *Macromolecules*, 2005, **38**, 8066-8070.
26. V. V. Lulevich, D. Andrienko and O. I. Vinogradova, *J. Chem. Phys.*, 2004, **120**, 3822-3826.
27. L. Han, L. Wang, K.-K. Chia, R. E. Cohen, M. F. Rubner, M. C. Boyce and C. Ortiz, *Adv. Mater.*, 2011, **23**, 4667-4673.
28. D. J. Schmidt, F. Ç. Cebeci, Z. I. Kalcioglu, S. G. Wyman, C. Ortiz, K. J. Van Vliet and P. T. Hammond, *ACS Nano*, 2009, **3**, 2207-2216.
29. A. M. Lehaf, H. H. Hariri and J. B. Schlenoff, *Langmuir*, 2012, **28**, 6348-6355.
30. S. T. Dubas and J. B. Schlenoff, *Langmuir*, 2001, **17**, 7725-7727.
31. J. A. Jaber and J. B. Schlenoff, *J. Am. Chem. Soc.*, 2006, **128**, 2940-2947.
32. D. J. Schmidt, Y. Min and P. T. Hammond, *Soft Matter*, 2011, **7**, 6637-6647.
33. A. Reisch, M. D. Moussallem and J. B. Schlenoff, *Langmuir*, 2011, **27**, 9418-9424.
34. O. Mermut, J. Lefebvre, D. G. Gray and C. J. Barrett, *Macromolecules*, 2003, **36**, 8819-8824.
35. L. Richert, A. J. Engler, D. E. Discher and C. Picart, *Biomacromolecules*, 2004, **5**, 1908-1916.
36. A. Schneider, G. Francius, R. Obeid, P. Schwinte, J. Hemmerle, B. Frisch, P. Schaaf, J. C. Voegel, B. Senger and C. Picart, *Langmuir*, 2006, **22**, 1193-1200.
37. R. A. Ghostine, M. Z. Markarian and J. B. Schlenoff, *J. Am. Chem. Soc.*, 2013, **135**, 7636-7646.

Soft Matter Accepted Manuscript

38. M. O. Lisunova, I. Drachuk, O. A. Shchepelina, K. D. Anderson and V. V. Tsukruk, *Langmuir*, 2011, **27**, 11157-11165.
39. F. Dubreuil, N. Elsner and A. Fery, *Eur. Phys. J. E*, 2003, **12**, 215-221.
40. D. Collin, P. Lavalle, J. M. Garza, J. C. Voegel, P. Schaaf and P. Martinoty, *Macromolecules*, 2004, **37**, 10195-10198.
41. J. A. Jaber and J. B. Schlenoff, *Chem. Mater.*, 2006, **18**, 5768-5773.
42. M. Safouane, R. Miller and H. Mohwald, *J. Colloid Interface Sci.*, 2005, **292**, 86-92.
43. J. Lukkari, M. Salomaki, T. Aaritalo, K. Loikas, T. Loiko, T. Laiho and J. Kankare, *Langmuir*, 2002, **18**, 8496-8502.
44. G. Francius, J. Hemmerle, V. Ball, P. Lavalle, C. Picart, J.-C. Voegel, P. Schaaf and B. Senger, *J. Phys. Chem. C*, 2007, **111**, 8299-8306.
45. H. H. Hariri, A. M. Lehaf and J. B. Schlenoff, *Macromolecules*, 2012, **45**, 9364-9372.
46. G. Francius, J. Hemmerle, J. Ohayon, P. Schaaf, J. C. Voegel, C. Picart and B. Senger, *Microsc. Res. Tech.*, 2006, **69**, 84-92.
47. P. J. Flory, in *Principles of Polymer Chemistry*, Cornell University Press, 1953, pp. 432-494.
48. M. C. Boyce and E. M. Arruda, *Math. Mech. Solids*, 2001, **6**, 641-659.
49. J. Choi and M. F. Rubner, *Macromolecules*, 2005, **38**, 116-124.
50. T. R. Farhat and J. B. Schlenoff, *J. Am. Chem. Soc.*, 2003, **125**, 4627-4636.
51. S. W. Cranford, C. Ortiz and M. J. Buehler, *Soft Matter*, 2010, **6**, 4175-4188.
52. I. M. Ward and J. Sweeney, in *An Introduction to the Mechanical Properties of Solid Polymers*, John Wiley & Sons, West Sussex, UK, 2nd edn., 2004, pp. 53-78.
53. Y. Hu, X. Zhao, J. J. Vlassak and Z. Suo, *Appl. Phys. Lett.*, 2010, **96**, 121904.
54. P. C. Hiemenz and R. Rajagopalan, in *Principles of Colloid and Surface Chemistry*, Marcel Dekker, New York, NY, 1997, ch. 11, pp. 499-533.
55. S. S. Shiratori and M. F. Rubner, *Macromolecules*, 2000, **33**, 4213-4219.
56. S. E. Burke and C. J. Barrett, *Langmuir*, 2003, **19**, 3297-3303.
57. J. E. Wong, F. Rehfeldt, P. Hanni, M. Tanaka and R. V. Klitzing, *Macromolecules*, 2004, **37**, 7285-7289.
58. S. Yamamoto, M. Ejaz, Y. Tsujii, M. Matsumoto and T. Fukuda, *Macromolecules*, 2000, **33**, 5602-5607.
59. Technical specifications of Dimension Icon Atomic Force Microscope. BrukerNano, Santa Barbara, CA.
60. P. H. Mott, J. R. Dorgan and C. M. Roland, *J. Sound Vibrat.*, 2008, **312**, 572-575.
61. J. L. Hutter and J. Bechhoefer, *Rev. Sci. Instrum.*, 1993, **64**, 1868-1873.
62. D. C. Lin, E. K. Dimitriadis and F. Horkay, *J. Biomech. Eng.*, 2007, **129**, 430-440.
63. L. Han, E. H. Frank, J. J. Greene, H.-Y. Lee, H.-H. K. Hung, A. J. Grodzinsky and C. Ortiz, *Biophys. J.*, 2011, **100**, 1846-1854.
64. M. Ahearne, Y. Yang, A. J. El Haj, K. Y. Then and K. K. Liu, *J. R. Soc. Interface*, 2005, **2**, 455-463.
65. E. K. Dimitriadis, F. Horkay, J. Maresca, B. Kachar and R. S. Chadwick, *Biophys. J.*, 2002, **82**, 2798-2810.
66. C. Zener, *Elasticity and Anelasticity of Metals*, Chicago University Press, Chicago, IL, 1948.
67. T. Y. Tsui, W. C. Oliver and G. M. Pharr, *J. Mater. Res.*, 1996, **11**, 752-759.
68. A. Bolshakov, W. C. Oliver and G. M. Pharr, *J. Mater. Res.*, 1996, **11**, 760-768.
69. D. Dean, L. Han, C. Ortiz and A. J. Grodzinsky, *Macromolecules*, 2005, **38**, 4047-4049.
70. H. Riegler and F. Essler, *Langmuir*, 2002, **18**, 6694-6698.
71. P. J. Flory, in *Principles of Polymer Chemistry*, Cornell University Press, 1953, pp. 541-594.
72. D. Dean, L. Han, A. J. Grodzinsky and C. Ortiz, *J. Biomech.*, 2006, **39**, 2555-2565.
73. M. Ye, D. Zhang, L. Han, J. Tejada and C. Ortiz, *Soft Matter*, 2006, **2**, 243-256.
74. M. D. Buschmann and A. J. Grodzinsky, *J. Biomech. Eng.*, 1995, **117**, 179-192.
75. J. T. Overbeek, *Prog. Biophys. Biophys. Chem.*, 1956, **6**, 57-84.
76. S. A. Sukhishvili and S. Granick, *J. Am. Chem. Soc.*, 2000, **122**, 9550-9551.
77. M. Doi and S. F. Edwards, in *The Theory of Polymer Dynamics*, Oxford University Press, New York, NY, 1986, pp. 218-288.

Soft Matter Accepted Manuscript

78. V. Y. Kramarenko, T. A. Ezquerra, I. Sics, F. J. Balta-Calleja and V. P. Privalko, *J. Chem. Phys.*, 2000, **113**, 447-452.
79. C. H. Porcel and J. B. Schlenoff, *Biomacromolecules*, 2009, **10**, 2968-2975.
80. P. J. Flory, in *Principles of Polymer Physical Chemistry*, Cornell University Press, 1953, pp. 595-639.
81. N. M. Alves, J. L. G. Ribelles, J. A. Gomez-Tejedor and J. F. Mano, *Macromolecules*, 2004, **37**, 3735-3744.
82. H. T. Nia, I. S. Bozchalooi, Y. Li, L. Han, H.-H. Hung, E. H. Frank, K. Youcef-Toumi, C. Ortiz and A. J. Grodzinsky, *Biophys. J.*, 2013, **104**, 1529-1537.
83. H. T. Nia, L. Han, I. S. Bozchalooi, P. Roughley, K. Youcef-Toumi, A. J. Grodzinsky and C. Ortiz, *ACS Nano*, 2015, **9**, 2614-2625.
84. J. P. Gong, Y. Katsuyama, T. Kurokawa and Y. Osada, *Adv. Mater.*, 2003, **15**, 1155-1158.
85. L. Han, A. J. Grodzinsky and C. Ortiz, *Annu. Rev. Mater. Res.*, 2011, **41**, 133-168.
86. A. Rothen, *Rev. Sci. Instrum.*, 1945, **16**, 26-30.
87. G. H. Cross, A. A. Reeves, S. Brand, J. F. Popplewell, L. L. Peel, M. J. Swann and N. J. Freeman, *Biosens. Bioelectron.*, 2003, **19**, 383-390.
88. W. J. Okkerse, S. P. Ottengraf and B. Osinga-Kuipers, *Biotechnol. Bioeng.*, 2000, **70**, 619-629.
89. J. W. Wood and R. D. Redin, *Rev. Sci. Instrum.*, 1993, **64**, 2405-2406.
90. J. B. Theeten and D. E. Aspnes, *Ann. Rev. Mater. Sci.*, 1981, **11**, 97-122.
91. J. Ahn, T. Crouzier, K. Ribbeck, M. F. Rubner and R. E. Cohen, *Biomacromolecules*, 2015, **16**, 228-235.

Soft Matter Accepted Manuscript

Figure Captions

Fig. 1 Layer-by-layer (LbL) assembled poly(allylamine hydrochloride)/poly(acrylic acid) (PAH/PAA) PAH/PAA material model system. (a) pH-governed molecular state changes of PAH and PAA. (b) Schematic of the pH and ionic strength (IS)-dependent molecular organization of the ionically cross-linked PAH/PAA networks.

Fig. 2 pH and IS-dependent film thickness, H, of $(PAH7.5/PAA3.5)_{50}$ LbL films using two methods. (a) Schematics of methods I and II for the measurement of H. Method I: contact mode AFM imaging for $H < 10$ μm. Method II: the z-motor assisted method for $H \geq 10$ μm, including three steps: 1) Indentation on the film up to a pre-set force yielded the z-step motor movement distance, z_1, 2) the probe tip was laterally moved to over the surface of substrate via the x/y-step motor, 3) Ramp on the substrate yielded the z-step motor movement distance, z_2. The film thickness, H, was calculated as $H = z_2 - z_1 + D$, where D is the indentation depth at the pre-set force. (b) Height sensor outcome of one typical contact AFM imaging on the film with selective removal region shows the measurement of H by method I. (c) Comparison of H measured by methods I and II at 0.01M, pH 3.0 yielded no statistical differences ($p > 0.05$ via Mann-Whitney U test). (d) Film thickness, H, and associated swelling ratio, v_s, at all tested pH and IS (mean ± SEM for $n \geq 15$ measurements on at least three samples at each condition). The dashed line represents the dry film thickness (SEM is less than the line width).

Fig. 3 Effects of pH and IS on the instantaneous indentation modulus, E_0, of $(PAH7.5/PAA3.5)_{50}$ LbL films via AFM-based nanoindentation. (a) Typical indentation force versus depth (F-D) curves at different pH and IS (mean ± STD of ≥ 10 positions for each curve). The density of experimental data was reduced to increase clarity, and the solid line represents the least square linear regression fit of substrate-corrected Hertz model.[65] (b) Instantaneous indentation modulus calculated from F-D curves, E_0, of $(PAH7.5/PAA3.5)_{50}$ at various pH and IS (mean ± SEM for $n \geq 15$ positions on at least three samples). All experiments were performed at 5 μm/s constant indentation depth rate by a microspherical tip ($R \approx 12.5$ μm).

Fig. 4 Effects of pH and IS on the concomitant changes in modulus E_0 and film thickness H of $(PAH7.5/PAA3.5)_{50}$ LbL films. (a) The network switches from highly cross-linked, net neutral to much less cross-linked, net changed state from pH 5.5 to 2.0 at 0.01M IS, showing by ≈ 3.2 ± 0.1 × (mean ± SEM) increase in H and ≈ 135.6 ± 4.8 × reduction in E_0. (b) The network switches from highly cross-linked, net neutral to less cross-linked, net neutral state from 0.01M to 1.0M at pH 5.5, showing by ≈ 22.0 ± 0.4 % decrease in H and ≈ 9.0 ± 2.0 × reduction in E_0 (mean ± SEM, $n \geq 15$, *: $p < 0.0001$ via Mann-Whitney U test).

Fig. 5 AFM-based force relaxation measurement of $(PAH7.5/PAA3.5)_{50}$ at constant indentation depth. (a) Schematic of five-element standard linearized solid model implementing two viscoelastic relaxation time constants, τ_1 and τ_2, where instantaneous modulus, $E(t) = E_\infty + E_1\exp(-t/\tau_1) + E_2\exp(-t/\tau_2)$. (b) Typical normalized $E(t)$ versus initial indentation modulus, E_0, curves showing distinctive relaxation behaviors at different pH and IS of PAH/PAA. Dashed lines are the SLS model fit by non-linear least squares regression via the Levenberg-Marquardt algorithm (LMA).

Fig. 6 Degree of viscoelastic relaxation, shown as the ratio of equilibrium modulus, E_∞, versus instantaneous modulus E_0 of $(PAH7.5/PAA3.5)_{50}$. (a) Impacts of pH and IS on E_∞/E_0, and the associated degree of relaxation, $(1 - E_\infty/E_0)$ (mean ± SEM, $n \geq 15$, *: $p < 0.001$ via Mann-Whitney U test showing markedly higher elastic portion at pH 2.0, 0.01M compared with all other conditions). (b,c) Replot of the degree of relaxation versus (b) film thickness, H, and (c) instantaneous modulus, E_0 (mean ± SEM, $n \geq 15$, to increase clarity, data are shown for pH 5.5, 3.5, 2.5 at all IS, and pH 2.0 at 0.01M).

Fig. 7 Viscoelastic relaxation at both shorter (a,b) and longer (c,d) time domains at different pH and IS, predicted by the five-element SLS model. (a) E_1 and (c) E_2 normalized by initial modulus, E_0, and corresponding time constants (b) τ_1 and (d) τ_2, where E_1 corresponds to the greater degree of relaxation (mean ± SEM, $n \geq 15$, *: $p < 0.001$ via Mann-Whitney U test showing significantly different short term relaxation trends at pH 2.0, 0.01M compared with all other conditions).

Soft Matter Accepted Manuscript

Fig. 1

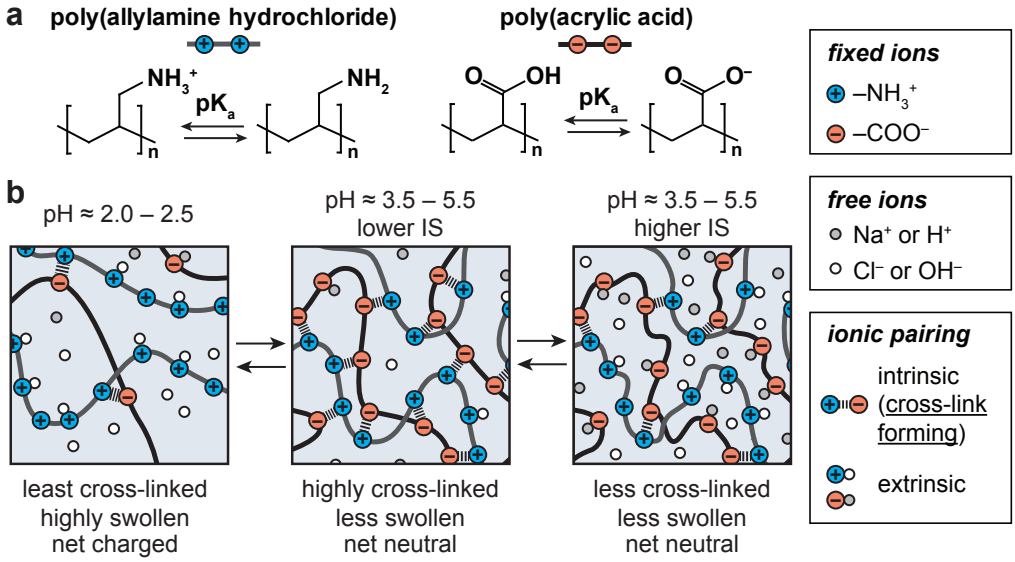

Soft Matter Accepted Manuscript

Fig. 2

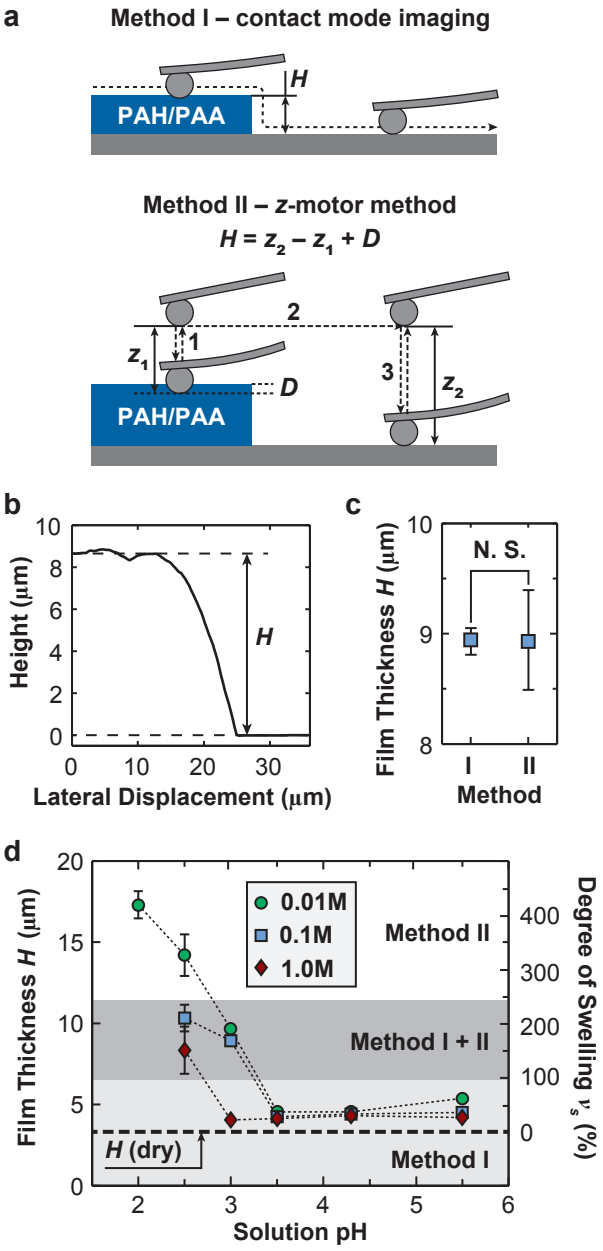

Soft Matter Accepted Manuscript

Fig. 3

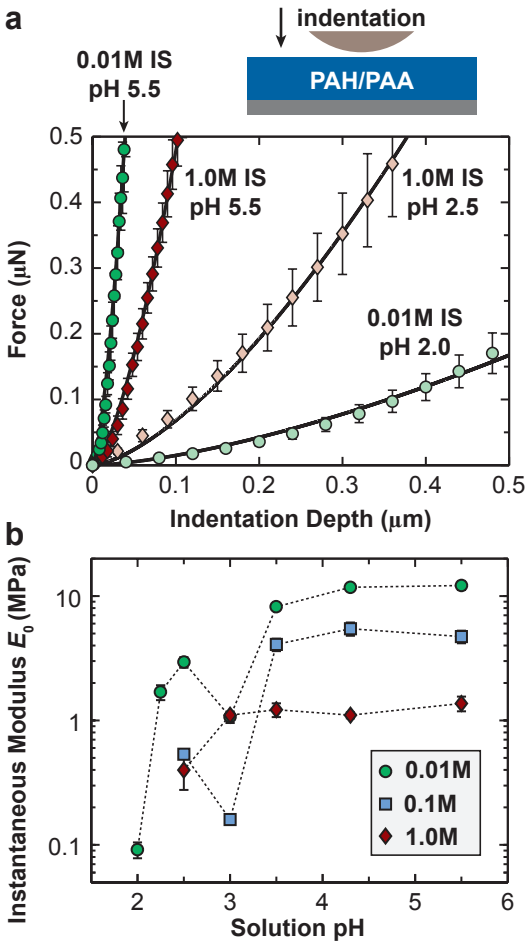

Soft Matter Accepted Manuscript

Fig. 4

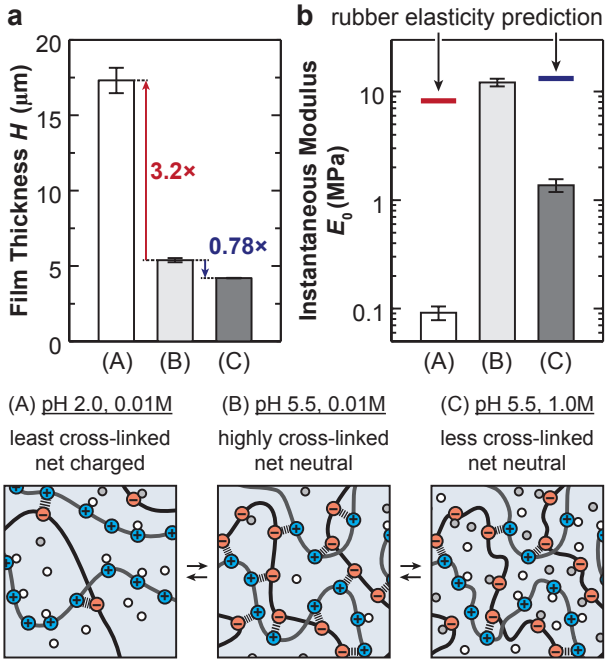

Soft Matter Accepted Manuscript

Fig. 5

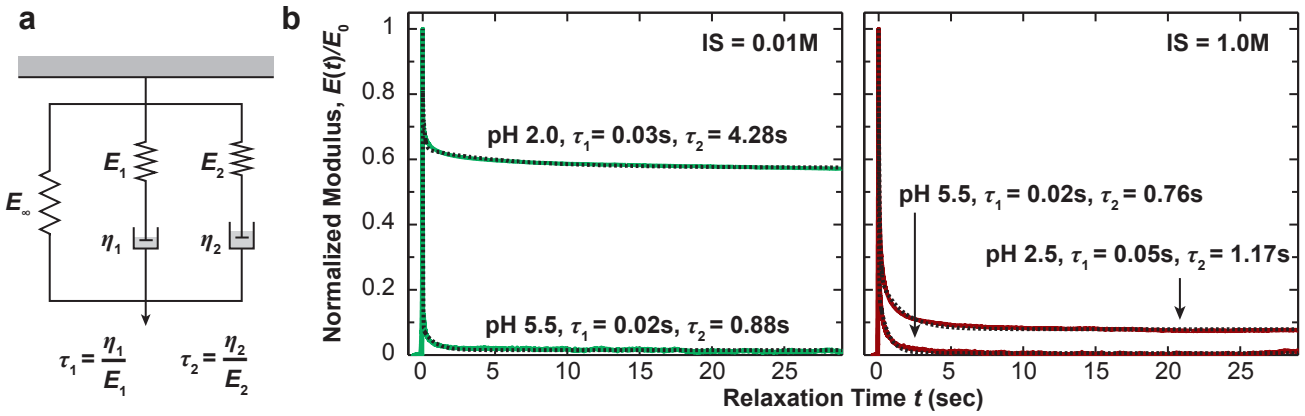

Soft Matter Accepted Manuscript

Fig. 6

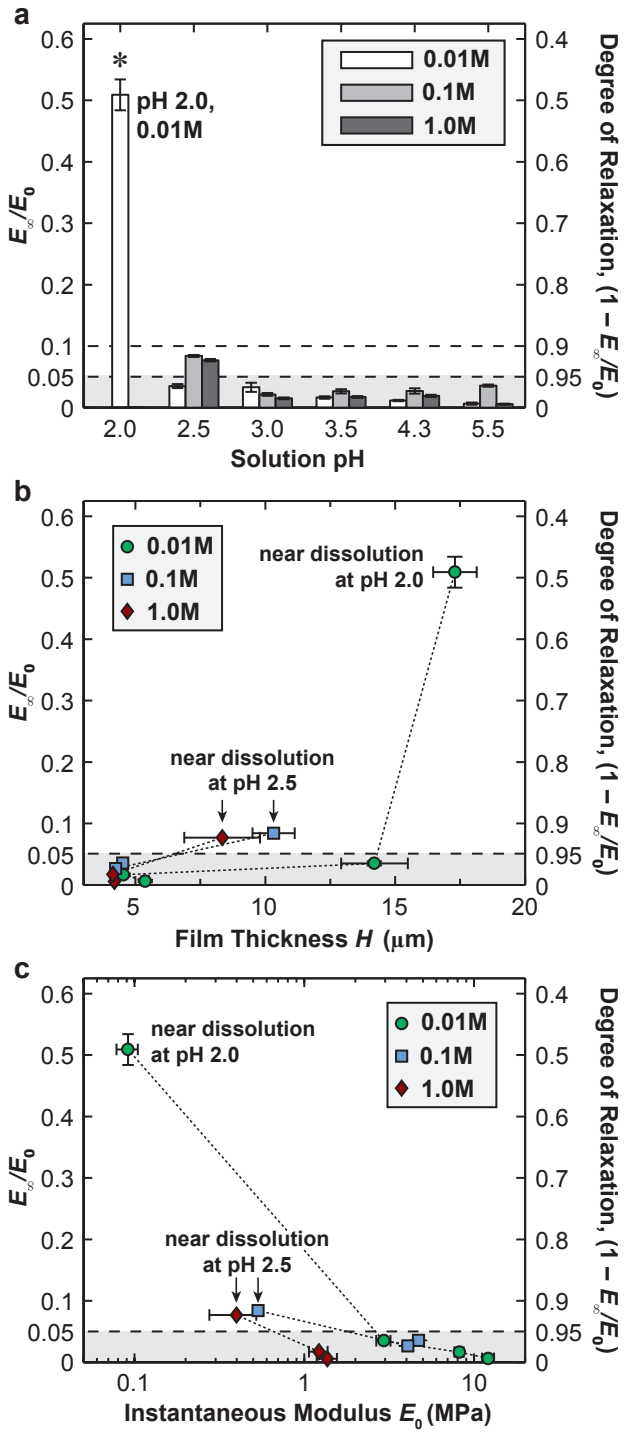

Soft Matter Accepted Manuscript

Fig. 7

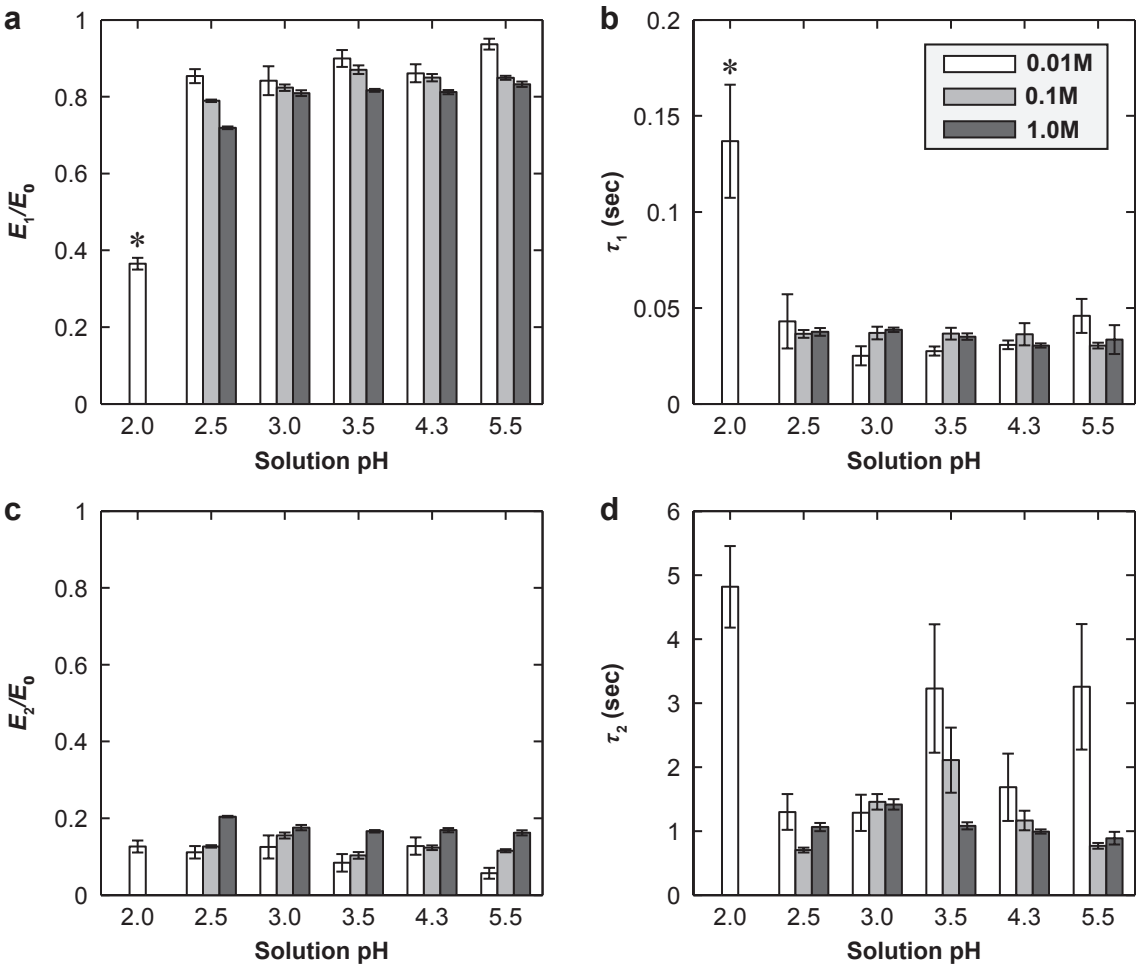

Soft Matter Accepted Manuscript

Table of Content

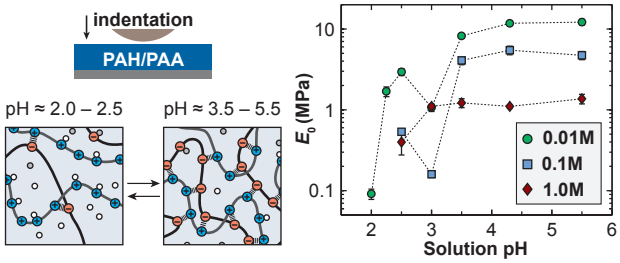

Soft Matter Accepted Manuscript